MRS Advances © 2017 Materials Research Society
DOI: 10.1557/adv.2017.379

Palladium Germanides for Mid- and Long-Wave Infrared Plasmonics

Evan M. Smith[1,2*], William H. Streyer[3], Nima Nader[2,4], Shivashankar Vangala[2,5], Richard Soref[6], Daniel Wasserman[7], and Justin W. Cleary[2]
[1]KBRwyle, Beavercreek, OH, 45431, USA
[2]Air Force Research Laboratory, Sensors Directorate, Wright-Patterson Air Force Base, Ohio, 45433, USA
[3]Department of Electrical and Computer Engineering, University of Illinois, Urbana-Champaign, IL, 61801, USA
[4]Solid State Scientific Corporation, Nashua, NH 03060, USA
[5]Azimuth Corporation, Dayton, OH 45431, USA
[6]The Engineering Program, University of Massachusetts at Boston, MA 02125, USA
[7]Department of Electrical and Computer Engineering, University of Texas Austin, Austin, TX 78758, USA

ABSTRACT

Palladium germanide thin films were investigated for infrared plasmonic applications. Palladium thin films were deposited onto amorphous germanium thin films and subsequently annealed at a range of temperatures. X-ray diffraction was used to identify stoichiometry, and Scanning Electron Micrographs, along with Energy Dispersive Spectroscopy (EDS) was used to characterize composition and film quality. Resistivity was also measured for analysis. Complex permittivity spectra were measured from 0.3 to 15 µm using IR ellipsometry. From this, surface plasmon polariton (SPP) characteristics such as propagation length and mode confinement were calculated and used to determine appropriate spectral windows for plasmonic applications with respect to film characteristics. Films were evaluated for use with on-chip plasmonic components.

INTRODUCTION

Plasmonic devices utilize sub-wavelength structures to confine and guide electromagnetic waves along the interface between dielectric and conductive media. Plasmonic waveguides enable the propagation of surface plasmon polaritons (SPP) based upon the structure geometry and the complex optical permittivity of the conductor. Applications include chemical and biological sensing, information processing, and integrated on-chip optoelectronic circuits [1-3]. Early research in plasmonics focused on noble metals due to their high conductivity and low loss. However, these materials are not useful in the infrared spectrum as their plasma frequency is typically in the UV or visible range [3, 4]. For mid-wave infrared (MWIR, 3-5µm) and long-wave infrared (LWIR, 8-12µm) applications, materials such as doped silicon and germanium [5, 6], transparent conducting oxides [7], metal silicides [5, 8] and metal germanides [9] have been investigated. A comprehensive review of these materials can be found in [2].

Metal silicides and metal germanides have been investigated extensively for their use as contact materials in transistor designs, and have been shown to have similar properties [10, 11]. This work seeks to expand upon the metal germanide system for plasmonic applications by studying palladium germanide films in a similar fashion to the Pt-Ge work presented in [9]. PdGe has been found to be stable over a wide temperature range and to have a low resistivity

[10], which makes it a good candidate as an SPP host material. Here, thin palladium films deposited on amorphous germanium are investigated as a function of anneal temperature. Film composition, texturing, and stoichiometry is characterized and correlated to resistivity and complex permittivity. Propagation length and mode confinement are calculated to determine the benefits of using PdGe films for MWIR and LWIR SPP waveguides.

EXPERIMENTAL PROCEDURES

Films were formed on p-type Si (100) wafers with vendor specified 0.001-0.005 ohm-cm resistivity. Substrates were cleaned in an O_2 plasma prior to deposition of materials. Electron beam evaporation was used to deposit 200 nm of germanium, followed by 50 nm palladium. Film thicknesses were measured by scanning electron microscope (SEM-Hitachi SU70) cross sectional imaging which confirmed a total thickness of 250 nm with a variation under 2%. Wafers were then diced into 1 cm^2 pieces which were annealed in a nitrogen purged tube furnace for 30 minutes each at temperatures between 300-500°C in 50°C intervals. Alternate samples were fabricated under identical processes to confirm repeatability.

Films were characterized by a variety of methods. X-ray diffraction (XRD, PANalytical Empyrean) using an asymmetric out-of-plane configuration was used to determine crystalline phase and stoichiometry. Surface morphology and structure were characterized by SEM imaging, and energy dispersive x-ray spectroscopy (EDS, EDAX) using a 10kV electron beam was used to determine relative film composition. Sheet resistance values were measured using a 4-point probe. Film resistivity was calculated as the product of the sheet resistance and the nominal film thickness (250 nm for the annealed films and 50 nm for unannealed Pd). Ellipsometry (J.A. Woollam, IR-VASE and V-VASE) was used to determine the complex optical constants for each film. For analysis, the annealed films were treated as a single 250 nm layer on the silicon substrate, and complex permittivity was determined using a Kramers-Kronig consistent model over the range of 300 nm- 15 μm using the Woollam WVASE32 software. A Drude term was used to fit the long-wave portion of the permittivity while Gaussian oscillators fit observed features at shorter wavelengths. For the unannealed sample, the model consisted of the 200 nm Ge layer and the 50 nm palladium layer.

CRYSTAL PROPERTIES

Analysis of the XRD data for the palladium germanide films indicates all films are polycrystalline material composed of a mixture of cubic Ge [PDF #01-089-4164] and orthorhombic PdGe [PDF #00-007-0286]. None of the identified peaks correspond strongly to the silicon substrate or to palladium silicide. Figure 1 presents the relative peak intensities for peaks associated with the identified Ge and PdGe references, as well as the full-width half maxima (FWHM) of those peaks. The relative intensity of the Ge (111) peak at 27.3° is fairly constant over this temperature range, while the peaks at 45.3° and 53.7°, corresponding to the (022) and (113) phases, respectively, show a slight decrease. Three of the PdGe peaks are greatly diminished as anneal temperature increases: 29.4° (011), 33.2° (111), and 41.7° (112). The PdGe (002) phase at 28.4°C increases, while the PdGe (103) peak at 46°C remains high, indicating a preferential texture of the material.

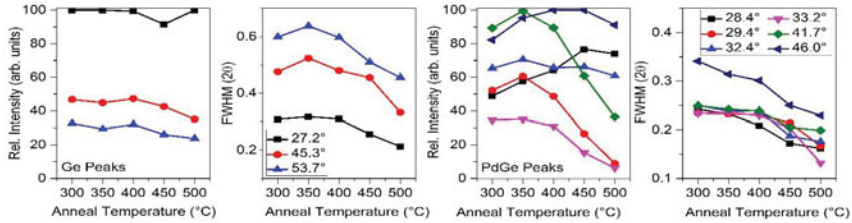

Figure 1. Relative intensity and Full Width Half Maximum (FWHM) of peaks from the XRD spectra. (Left) Peaks corresponding to Ge and (right) PdGe. (Full color online)

More significantly, all peaks uniformly become narrower with increased temperature, as the FWHM is reduced. Peak width is related to crystallite size by the Scherrer equation [12]. Based on the identified germanium peaks, the average Ge grain size for samples A-C (300-400°C anneals) is about 20 nm, but grows to an average of 28 nm for sample E (500°C anneal). The A-C PdGe grains have average size about 33 nm and grow to 44 nm for sample E. While the Scherrer equation only gives a lower limit for grain size, the trend indicates crystallite growth into larger structures at higher anneal temperatures.

Figure 2 shows SEM images comparing surface morphology of the annealed films, including an unannealed film for comparison. The unannealed film appears smooth and consists of uniform grains less than 50 nm in diameter. Annealing causes diffusion of the palladium and germanium films and facilitates crystal growth. Samples A-C all show similar features. Grains appear to be 100 nm in size separated by small voids. EDS indicates the Ge:Pd ratio to be 2-2.5 for each of these three films, which suggests only a slightly higher volume of Ge crystals to PdGe.

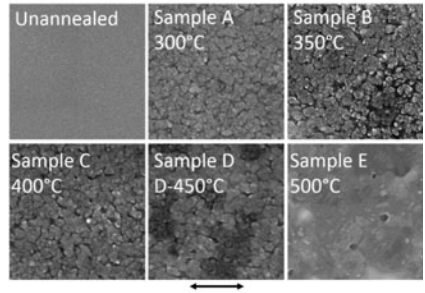

Figure 2. SEM images of annealed PdGe samples. All images have the same magnification.

The average grain size in sample D is larger, in agreement with the Scherrer calculation. Additionally, the film had been segregated into light and dark regions. EDS reveals the light regions have a similar Ge:Pd ratio of about 2.5, similar to films A-C. The dark regions, however, have a much higher concentration of germanium. In sample E the grains have grown together into a seemingly smooth surface. The voids that were present in all other films are no longer visible, and it is difficult to make a determination on grain size. Like sample D, this film has

dark and light regions; the light regions are a mixture of PdGe and Ge while the dark regions are mostly Ge.

The XRD and EDS data indicate that all films are a mixture of stoichiometric PdGe and Ge grains, and that these grains grow in size with higher anneal temperatures. Lower temperature annealing produces a mildly textured, rough film. At higher temperatures, films become highly textured with a preferred (111) orientation for Ge and (002) orientation for PdGe. The film, which is generally evenly mixed between Pd and Ge crystals has pockets of Ge-rich material.

These results agree with the conclusions of previous research. Hsieh and Chen formed palladium germanide films by depositing thin palladium films on Ge (111) and Ge (001) substrates, and observed Pd_2Ge as-deposited, while annealing between 250°C-500°C showed only PdGe [11]. They conclude that while other compounds of the palladium-germanium alloy exist in bulk systems, thin films only allow for PdGe and Pd_2Ge, the latter of which only forms at lower temperatures. Gaudet et al. also determined PdGe to be stable over a wide anneal temperature range (~330°C-740°C) after depositing 30 nm Pd onto 200 nm α-Ge [10]. The authors of both works do not discuss any indication of Ge crystallization; it is possible their films were more completely diffused, or alternatively that the authors determined that the Ge peaks were not relevant in discussing the phase of the alloy.

ELECTRICAL and OPTICAL PROPERTIES

The resistivity of thin palladium on germanium films was measured to be about 25 μΩ-cm prior to annealing. Sample A-C have a resistivity nearly 4 times as large, while sample D measured at about 180 μΩ-cm. The high resistivity is likely due to the dislocations visible in the SEM images and the varying palladium-rich and germanium-rich structures. The resistivity of sample E falls below all other annealed films at 75μΩ-cm, which is still three times higher than unannealed palladium. This film has a smoother surface, more uniform crystal structures, and larger grain sizes. These factors may contribute to the lower resistivity.

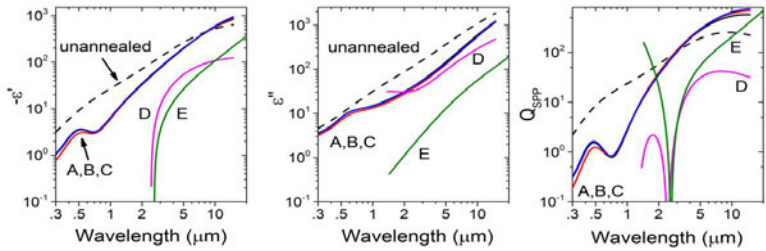

Figure 3. Measured (a) real and (b) imaginary parts of the permittivity for PdGe. (c) Q_{SPP} quality factor considered from [15] (Full color online)

Figure 3 (a) and (b) presents the modeled complex permittivity ε' and ε'' determined from ellipsometry measurements. All annealed films are assumed to be a single layer. Samples A-C are nearly indistinguishable, in agreement with the crystallographic similarities already discussed. Over the spectral range, the magnitude of ε' for sample E is higher than ε''; the opposite is true for sample D. In fact, ε'' is nearly 10 times smaller in sample E than for all other films. This low loss material is probably a result of the relatively smooth surface and the

preferred texture obtained after a high anneal. The observed ε' =0 point of both samples D and E is around 2.5 μm, with the latter being at a slightly longer wavelength. Samples D and E were not measured in the visible spectrum.

Determination of the complex permittivity allows for the calculation of SPP characteristics such as field penetration depth, which indicates the quality of the mode confinement, and the propagation length, which considers energy loss. The 1/e SPP field penetration depth from the interface into the dielectric (d) or conductor (c) is [13]

$$L_{d,c} = \left[\frac{2\pi}{\lambda}\mathrm{Re}\sqrt{-\frac{\epsilon_{d,c}^2}{\epsilon_d+\epsilon_c}}\right]^{-1}. \quad (1)$$

It is typical to calculate the field penetration into air for an SPP host material, therefore $\epsilon_d = 1$ in Eq. 1. The plasmon propagation length is given by [13]

$$L_x = [2\ \mathrm{Im}\ k_{SPP}]^{-1}, \quad (2)$$

where the SPP wavevector is

$$k_{SPP} = \frac{2\pi}{\lambda}\sqrt{\frac{\epsilon_d\epsilon_c}{\epsilon_d+\epsilon_c}}. \quad (3)$$

These equations are for a single interface. For our films the calculated penetration depth in the conductor, L_c in Eq. 1, is less then 250 nm for all, except for sample E at wavelengths where ε' is positive. For the unannealed film, L_c is less than 50 nm below 8μm. We therefore conclude that the films are sufficiently thick for the following analysis.

Standard quality factors or criteria are necessary to compare various materials. West et al. [14] suggest $Q_{SPP} = \frac{\epsilon'^2}{\epsilon''}$, which considers the field propagation length, plotted in Figure 3(c). This indicates that lower temperature annealing yeilds better energy propogation lengths. However, this does not consider limitations based upon mode confinement. On the other hand, Soref et al. [5] suggest that a SPP host material is useful only if the field penetration depth in the dielectric is sufficiently small and the propogation length is sufficiently large. They argue that the lower spectral limit is given by $L_x > 2\lambda$ while the upper spectral limit is when $L_d < 3\lambda$.

Based on this criteria we calculate the useful spectral range and present the results in Table 1. This is calculated using air as the dielectric (ε_d=1), and is meant to be representative of differences between the films. Using an alternate dielectric, such as germanium, would shift the spectral ranges to longer wavelengths, but the observed trend would remain the same. The useful range for the unannealed film occupies the shortest wavelengths. Low temperature anneals increase the spectral range, in this case to include the NIR and MWIR. Higher temperature anneals enhance the mode confinement and extend the useful spectral range into the LWIR. After a 450°C anneal, the spectral range is extended to 8.4μm, while the lower limit is below the ε'=0 point. Strictly speaking, this spectral range should not be called "plasmonic" as SPPs are generally said to be excited when ε'<0. However, it has been shown that bound electromagnetic surface waves can exist when the the real part of the permittivity is positive provided that ε'<<ε'' [15,16]. After a 500°C anneal, the PdGe film has the strongest mode confinement which extends the spectral range well beyond the LWIR, although propogation loss around the ε'=0 point limits the lower end of the useful spectral range.

Table 1. Predicted spectral range of a plasmonic waveguide for annealed PdGe films. Calculated range is based upon measured permittivity values.

Anneal Temperature [°C]	unannealed	300	350	400	450	500
SPP Spectral Range (μm)	0.44-3.7	0.7-5.7	0.8-5.9	0.7-5.8	1.4-8.4	3.3-17.7

SUMMARY

Ellipsometry, resistivity and XRD measurements all seem to show a similar trend. All films appear to be mixtures of PdGe and Ge; it is not evident from this work that anneal temperature changes the stoichiometry of the alloy for this temperature range. At lower temperature anneals, samples A-C are similar. After a 450°C anneal, the film separates into Pd-rich regions and Ge-rich regions, which causes the resistivity to increase and the magnitude of the complex permittivity to decrease. The XRD data suggests that while the crystal phase is unchanged, the texturing of the films changes to preferred phase orientations of larger-sized crystals. After a 500°C anneal, the film surface is smooth as grains have sufficiently grown to have very small grain boundaries, resulting in a low loss film with low resistivity. Samples A-C could operate for NIR and MWIR applications. Sample E would be ideal for working in both MWIR and LWIR applications, and its low resistivity makes it an attractive host material for optoelectronic applications.

ACKNOWLEDGEMENTS

This material is based upon work supported by the Air Force Office of Scientific Research under award number FA9550-15RYCOR162.

REFERENCES

1. R. Soref, Nat. Photonics **4**, 495-497 (2010).
2. G.V. Naik, V.M. Shalaev, A. Boltasseva, Adv. Mater. 25, 3264-3294 (2013).
3. S. Lal, S. Link, N. Halas, Nat. Photonics, **1**, 641-648, (2007).
4. S. Maier, *Plasmonics: Fundamentals and Applications* (Springer, New York, 2007).
5. R. Soref, R.E. Peale, and W. Buchwald, Opt. Express **16**(9), 6507-6414 (2008).
6. R. Soref, J. Hendrickson, J.W. Cleary, Opt. Express **20**(4), 3814-3824 (2012).
7. J.W. Cleary, M.R. Snure, K.D. Leedy, D.C Look, K. Eyink, A. Tiwari, Proc. SPIE **8545**, 854504 (2012).
8. J.W. Cleary, R.E. Peale, D.J. Shelton, G.D. Boreman, C.W. Smith, M. Ishigami, R. Soref, A. Drehman, W.R. Buchwald, J. Opt. Soc. Am. B, **27**(4), 730-734, (2010).
9. J.W. Cleary, W.H. Streyer, N. Nader, S. Vangala, I. Avrutsky, B. Claflin, J. Hendrickson, D. Wasserman, R.E. Peale, W. Buchwald, R. Soref, Opt. Express **23**(3), 3316-3326 (2015).
10. S. Gaudet, C. Detavernier, A.J. Kellock, P. Desjardins, and C. Lavoie, J. Vac. Sci. Technol. **24**(3), 474-485 (2006).
11. Y.F. Hsieh and L.J. Chen, Thin Solid Films, **162**, 295-303 (1988).
12. A. Patterson, Phys. Rev. **56**, 978 (1939).
13. H. Raether, *Surface Plasmons on Smooth and Rough Surfaces and on Gratings* (Springer, Berlin Heidelberg, 1988) pp. 4-7.
14. P.R. West, S. Ishii, G.V.Naik, N.K. Emani, V.M. Shalaev, A. Boltasseva, Laser Photonics Rev. 4(**6**), 795-808 (2010).
15. J.W. Cleary, G. Medhi, M. Shahzad, I. Rezadad, D. Maukonen, R.E. Peale, G.D. Boreman, S. Wentzell, W.R. Buchwald, Opt. Express **20**(3), 2693-2705 (2012).
16. F. Yang, J.R. Sambles, and G.W. Bradberry, Phys. Rev. B Condens. Matter **44**(11), 5855-5872 (1991).